Supporting Information

Matos et al. 10.1073/pnas.1119075109

SI Materials and Methods

Plasmids. PCR fragments for T7-tagged constructs encoding the indicated residues of Mint1 or Mint2 were subcloned into pET-28a (Novagen): pET/Mint1 453–635, Mint1 453–643, Mint1 453–749, Mint1 453–824, Mint1 453–839, Mint1 220–321, Mint1 1–635, Mint1 1–643, Mint1 1–645, Mint1 1–659, Mint1 1–839; pET/Mint2 363–546, Mint2 363–554. For NMR, isothermal titration calorimetry (ITC), and crystallography, PCR fragments encoding the indicated residues of Mint1 were subcloned into a modified pGEX-KG vector containing a tobacco etch virus (TEV) protease cleavage site: pGEX-TEV/Mint1 453–635, Mint1 453–643, Mint 453–635*, Mint1 453–643* (* lacking residues 499–508, 569–585). Mint1 point mutants (Tyr633 to -Ala, -Glu, -Phe) were generated by QuickChange Site Directed Mutagenesis (Stratagene). EGFP-tagged *cre*-recombinase and Mint1 were expressed simultaneously from a bicistronic lentiviral vector and were produced as described (1). Briefly, lentiviral vectors contained an EGFP-*cre*-recombinase 5′ open reading frame with a downstream internal ribosome entry site sequence followed by the Mint1 open reading frame of Mint1 453–839 with and without the Y633A mutation.

Expression and Affinity purification of Mint Fusion Proteins. Mint fusion proteins were expressed in BL21 (DE3) strain of *Escherichia coli*. For T7-tagged Mints, bacterial pellets were resuspended in ice-cold PBS with protease inhibitors and sonicated. Triton X-100 was added to 1%, and cleared by centrifugation at 14,000 × *g* for 20 min at 4 °C. Lysates were treated with bezonase (Novagen; 25 units/mL lysate, supplemented with 2 mM $MgCl_2$) for 2 h at room temperature. β-Mercaptoethanol was added to 2 mM and proteins immunoaffinity purified on T7 antibody-coupled agarose (Novagen). ^{15}N-labeled proteins for NMR studies were expressed in minimal media using $^{15}NH_4Cl$ as the sole nitrogen source. For ITC, NMR, and crystallography studies, bacterial pellets were resuspended in ice-cold PBS buffer supplied with 5 mM dithiothreitol, 0.2 mM 4-(2-aminoethyl)benzenesulfonyl fluoride, and quick frozen in liquid N_2. Cells were thawed on ice and broken by passing through Avestin Homogenizer three times at >12,000 psi. After centrifugation at 16,000 × *g* for 30 min, the supernatant was incubated with Glutathione Sepharose 4B resin (GE Healthcare) for 2 h at 4 °C. The resin was washed sequentially with PBS, PBS containing 1% Triton X-100, PBS containing 1M NaCl, PBS, and TEV cleavage buffer (50 mM Tris, pH 8.0, 0.1 M NaCl), cleaved from the GST moiety by TEV, and purified by ion-exchange and size-exclusion chromatography.

Antibodies. N-terminal 22C11 amyloid precursor protein (APP) antibody (MAB348) was obtained from Millipore, APP-like protein (APLP) -1 (171615) and -2 (171616) antibodies from Calbiochem, Mint2 (611033) from BD Transduction Laboratories, Mint3 (PA1-072) from Pierce, and the T7 antibody (69522) from Novagen. C-terminal APP (U955), Mint1 (P730), and EGFP (T3743) antibodies have been previously described (2, 3, 4).

Phase Determination and Structure Refinement. Phases for the phosphotyrosine binding (PTB*) domain were obtained from a single-wavelength sulfur anomalous dispersion experiment using native protein with data to a d_{min} of 1.90 Å. Data for structure solution were collected from two crystals. The first crystal diffracted to higher resolution, but had a high level of systematic errors due to uneven rotation of the spindle axis. The second crystal diffracted to a somewhat lower resolution, but all types of systematic errors were lower. The anomalous signal was estimated by merging anomalous signals from datasets obtained from these two crystals. Applying a correction for uneven spindle rotation (5) was essential to locate the heavy atom positions. Another important calculation required for optimal structure solution involved correcting for effects resulting from radiation damage (6) and calculating an optimal error model. Despite the use of a laboratory X-ray source, the level of radiation damage for the first crystal was close (within a factor of two) to the limit at which high-resolution data decay to immeasurable levels. Crystals exhibited moderate levels of anisotropy (Table S1), which was corrected by anisotropic sharpening. SHELXD (7) was used to find 12 heavy atom positions with a resulting correlation coefficient of 32.9% to 2.7 Å. The sites represented 10 out of 10 possible sulfur sites, plus one site with an alternate conformation and one partial-occupancy chloride ion. Initial phases were calculated and refined with the program MLPHARE (8) resulting in an overall figure-of-merit (FOM) of 0.21 to 2.7 Å, and FOM = 0.26 for acentric reflections. Phases were further improved by cycles of alternating density modification with the program Parrot (9) and model building with the program Buccaneer (10), followed by model building with the program ARP/wARP (11). The resulting model contained 75% of all Mint1 (residues 453–643). Additional residues were manually modeled in the program Coot (12). Refinement was performed versus a dataset obtained from a single PTB* domain crystal, processed and scaled with Bijvoet pairs merged, using the program PHENIX (13) with a random 5% of all dataset aside for an R_{free} calculation. The current model contains 87.4% of all residues in the PTB* domain monomer; included are residues 455–496, 514–620, 623–640, one chloride ion, two acetate ions, two isopropanols, two glycerols, and 78 waters. The working R factor is 0.197 and the free R factor is 0.225. A Ramachandran plot generated with Molprobity (14) indicated that 100% of all protein residues are in the favored regions. Model refinement statistics are in Table S1.

Cortical Cultures and Lentiviral Infection. Dissociated high-density neocortical cultures were prepared from newborn mice as described previously (3, 15) and dissociated with trypsin for 5 min at 37 °C, triturated, and plated onto Matrigel coated plates. Neurons were maintained in culture at 37 °C in a humidified incubator with 95% air and 5% CO_2. Recombinant lentiviruses were produced by transfecting HEK293T cells with plasmids for viral enzymes and envelope proteins with FuGENE (Roche) as previously described (3, 15). Lentivirus-containing culture medium was harvested 48 h later, centrifuged at 1,000 × *g* for 10 min, and immediately added to neurons at 3–4 d in vitro (DIV) and analyzed at 14–16 DIV.

Aβ Peptide Measurement. Conditioned media was collected from neuronal cultures and centrifuged at 16,000 × *g* for 5 min at 4 °C and the supernatant was used for ELISA. ELISAs were performed according to the instructions provided by the manufacturer's protocol (Immunobiological Laboratories Kit for human Aβ42, 27711). Significance determined by one way ANOVA with post hoc Tukey–Kramer multiple comparisons test.

1. Kaeser PS, et al. (2009) ELKS2alpha/CAST deletion selectively increases neurotransmitter release at inhibitory synapses. *Neuron* 64:227–239.

2. Okamoto M, Südhof TC (1997) Mints, Munc18-interacting proteins in synaptic vesicle exocytosis. *J Biol Chem* 272:31459–31464.

3. Ho A, et al. (2006) Genetic analysis of Mint/X11 proteins: Essential presynaptic functions of a neuronal adaptor protein family. *J Neurosci* 26:13089–13101.
4. Han W, et al. (2004) N-glycosylation is essential for vesicular targeting of synaptotagmin 1. *Neuron* 41:85–99.
5. Otwinowski Z, Borek D, Majewski W, Minor W (2003) Multiparametric scaling of diffraction intensities. *Acta Crystallogr A* 59:228–234.
6. Borek D, Cymborowski M, Machius M, Minor W, Otwinowski Z (2010) Diffraction data analysis in the presence of radiation damage. *Acta Crystallogr D Biol Crystallogr* 66:426–436.
7. Schneider TR, Sheldrick GM (2002) Substructure solution with SHELXD. *Acta Crystallogr D Biol Crystallogr* 58:1772–1779.
8. Otwinowski Z (1991) Maximum likelihood refinement of heavy atom parameters. *Isomorphous Replacement and Anomalous Scattering*, eds Wolf W, Evans PR, Leslie AGW (Science and Engineering Research Council, Cambridge, UK), pp 80–86.
9. Zhang KY, Cowtan K, Main P (1997) Combining constraints for electron-density modification. *Methods Enzymol* 277:53–64.
10. Cowtan K (2006) The Buccaneer software for automated model building. 1. Tracing protein chains. *Acta Crystallogr D Biol Crystallogr* 62:1002–1011.
11. Langer G, Cohen SX, Lamzin VS, Perrakis A (2008) Automated macromolecular model building for X-ray crystallography using ARP/wARP version 7. *Nat Protoc* 3:1171–1179.
12. Emsley P, Cowtan K (2004) Coot: Model-building tools for molecular graphics. *Acta Crystallogr D Biol Crystallogr* 60:2126–2132.
13. Adams PD, et al. (2002) PHENIX: Building new software for automated crystallographic structure determination. *Acta Crystallogr D Biol Crystallogr* 58:1948–1954.
14. Davis IW, et al. (2007) MolProbity: All-atom contacts and structure validation for proteins and nucleic acids. *Nucleic Acids Res* 35:W375–383.
15. Ho A, Liu X, Südhof TC (2008) Deletion of Mint proteins decreases amyloid production in transgenic mouse models of Alzheimer's disease. *J Neurosci* 28:14392–14400.

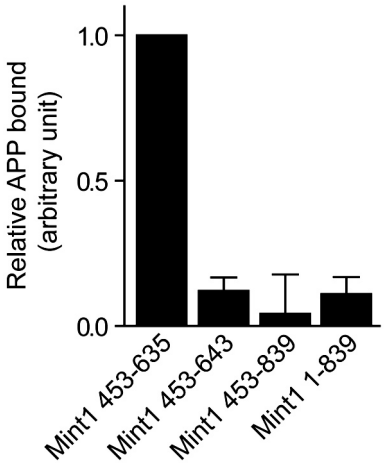

Fig. S1. Quantification of Mint1 interactions with APP. C-terminal extension of Mint1 PTB domain and full-length Mint1 exhibited significantly decreased binding to APP relative to Mint1 453–635.

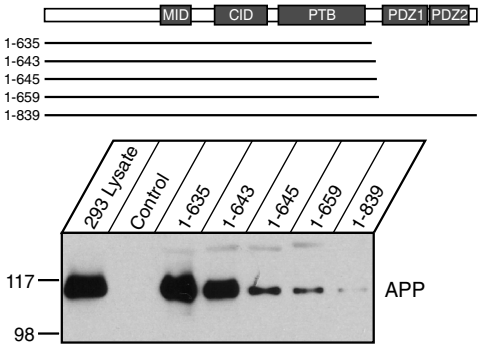

Fig. S2. Schematic of rat Mint1 recombinant proteins. Numbers on the left indicate amino acid positions. Western blot analysis of APP from transiently transfected HEK293T cells bound to full-length and progressive C-terminally truncated Mint1 proteins. MID, Munc18 interacting domain; CID, CASK interacting domain; PDZ, postsynaptic density-95/Discs large/zona occludens-1.

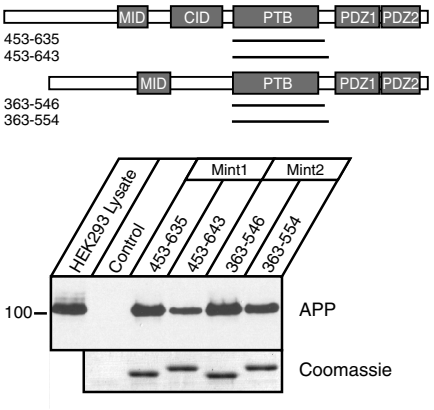

Fig. S3. Western blot analysis of APP from transiently transfected HEK293T cells bound to the different Mint1 and Mint2 recombinant proteins. Lower panel shows Coomassie stained gel of T7-tagged Mint proteins. MID, Munc18 interacting domain; CID, CASK interacting domain; PDZ, postsynaptic density-95/Discs large/zona occludens-1.

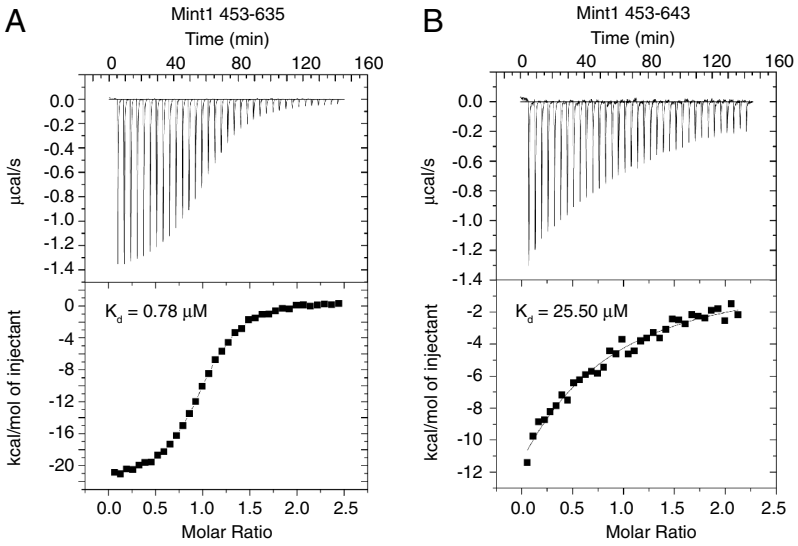

Fig. S4. Illustrative examples of ITC data obtained for binding of the APP peptide to the Mint1 PTB domain (*A*; residues 453–635) and Mint1 PTB domain including the linker region (*B*; residues 453–643).

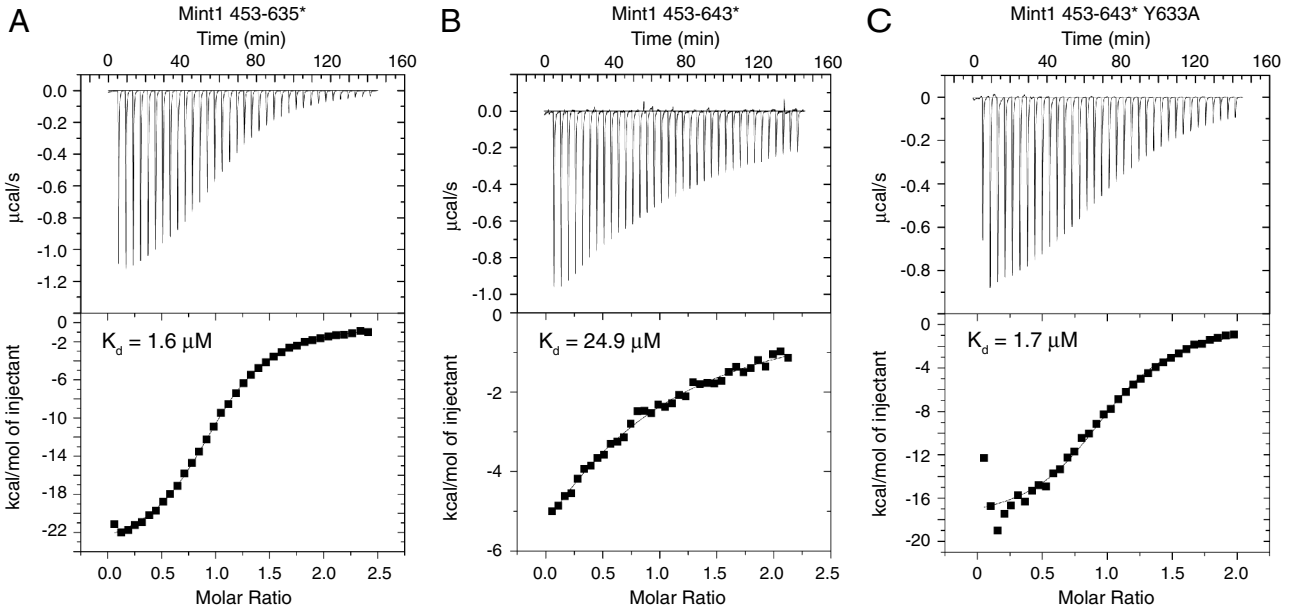

Fig. S5. Illustrative examples of ITC data obtained for binding of the APP C-terminal peptide to Mint1 fragments with the loop deletions and spanning the PTB* domain (*A*; Mint1$^{453–635*}$) or the PTB* domain with the C-terminal extension without (*B*; Mint1$^{453–643*}$) or with the Y633A mutation (*C*; Mint1$^{453–643*}$ Y633A).

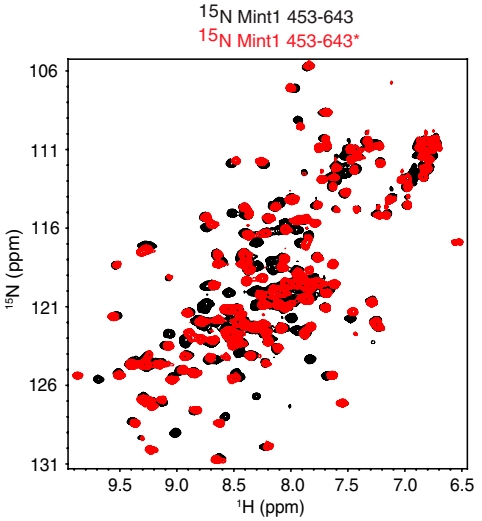

Fig. S6. The overall structure of the Mint1 PTB domain is preserved after removing the loops. A superposition of ^{1}H-^{15}N heteronuclear single quantum coherence spectra of Mint1$^{453–643}$ (black) and Mint1$^{453–643*}$ (red) is shown. The cross-peaks of Mint1$^{453–643*}$ coincide with or are near a cross-peak from Mint1$^{453–643}$, showing that the overall structure of the domain is not affected by removal of the loops. The additional black cross-peaks from Mint1$^{453–643}$ can be attributed to residues from the loops that were removed.

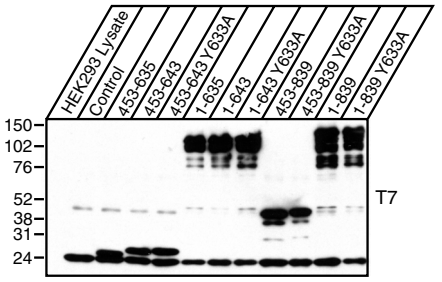

Fig. S7. Western blot analysis of T7-tagged Mint1 proteins from a pull-down experiment performed with HEK293T cells overexpressing APP.

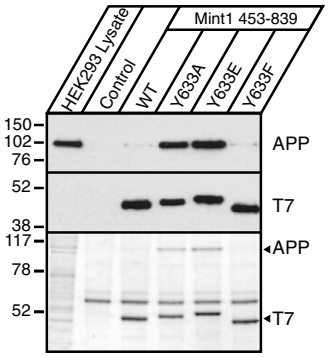

Fig. S8. Mint1 C-terminal fusion proteins (residues 453–839) with Tyr633 substitutions to alanine (Y633A), glutamic acid (Y633E), or phenylalanaine (Y633F) were incubated with lysates from APP overexpressing HEK293T cells and bound protein probed for APP and T7-tagged Mint1 proteins. Lower panel shows Coomassie stained gel of T7-tagged Mint proteins.

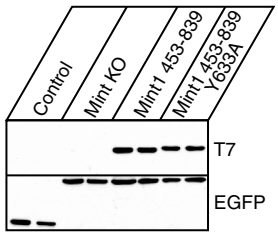

Fig. S9. Western blot analyses for T7 (Mint1 expression) and EGFP (*cre* expression) from HEK293T cells. Comparable internal ribosome entry site-dependent expression of the Mint1 C terminus ($Mint1^{453–839}$) with and without the Y633A mutation that was used to infect neurons shown in Fig. 5.

Table S1. Data collection, phasing, and refinement statistics

Data collection		
	Crystal I	Crystal II
Space group	$P4_12_12$	$P4_12_12$
Wavelength, Å	CuKα	CuKα
Resolution range, Å	35.83–1.90 (1.92–1.90)	50.00–2.00 (2.02–2.00)
Unique reflections	19,927 (467)	16,864 (329)
Multiplicity	13.6 (11.5)	9.4 (3.8)
Data completeness, %	99.5 (97.9)	98.0 (78.1)
R_{merge},* %	6.6 (95.7)	4.6 (62.9)
$I/\sigma(I)$	42.2 (2.3)	44.3 (2.0)
Wilson B value, Å^2	27.6	28.1
Phase determination		
Anomalous scatterers	sulfur, 10 sites refined as 12 positions	
Figure of merit (35–2.7 Å), %	0.269 (acentric reflections) 0.210 (all reflections)	
Significant parameters related to phasing		
Increase of scaling B factor during data collection, Å^2	4.3	1.6
Anisotropy in diffraction between directions [00l] and [h00], [0k0], Å^2	+5.3	+3.4
Range of absorption correction, %	−36 to 38	−17 to 18
Rms of residual multiplicative error, %	2.3	1.4
Range of uneven rotation speed, %	−27 to 25	−16 to 14
Rms of uneven rotation speed, %	5.5	3.0
Δ**F**/**F** representing specific radiation damage, %	17	9.6
$\mathbf{F}_a$/**F** representing phasing signal, %	1.1	1.1
Refinement statistics		
Crystal	Crystal I	
Resolution range, Å	33.02–1.90 (2.00–1.90)	
No. of reflections R_{work}/R_{free}	18,378 (1,351)/934 (61)	
Data completeness, %	92.1 (51.0)	
Atoms (non-H protein/water/solvent)	1,203/78/29	
R_{work}, %	19.7 (19.7)	
R_{free}, %	22.5 (24.4)	
Rmsd bond length, Å	0.017	
Rmsd bond angle, °	1.44	
Mean B value, Å^2 (protein/water/solvent)	54.9/46.1/55.3	
Ramachandran plot, % (favored/additional/disallowed)†	95.2/4.8/0.0	
Maximum likelihood coordinate error	0.42	
Missing residues	453–454, 497–513, 621–622, 641–643	

Data for the outermost shell are given in parentheses.

*$R_{merge} = 100\Sigma_h\Sigma_i|I_{h,i} - \langle I_h\rangle|/\Sigma_h\Sigma_i I_{h,i}$, where the outer sum ($h$) is over the unique reflections and the inner sum (i) is over the set of independent observations of each unique reflection.

†As defined by the validation suite MolProbity (1).

1. Davis IW, et al. (2007) MolProbity: All-atom contacts and structure validation for proteins and nucleic acids. *Nucleic Acids Res* 35:W375–383.